PLASMA SPECTROSCOPY

R.J.E. Jaspers
Science and Technology of Nuclear Fusion, Applied Physics, Eindhoven University of Technology
P.O. Box 513, 5600 MB Eindhoven, The Netherlands

ABSTRACT

A brief introduction into the spectroscopy of fusion plasmas is presented. Basic principles of the emission of ionic, atomic and molecular radiation is explained and a survey of the effects, which lead to the population of the respective excited levels, is given. Line radiation, continuum radiation, opacity and line broadening mechanisms are addressed. To access the core of a fusion reactor, active spectroscopic techniques have been developed, of which charge exchange recombination spectrosopy and Thomson scattering are treated in some detail.

I. INTRODUCTION

The beauty of a plasma relies in its optical emission: being it the Aurora Borealis, a lightning stroke or even the sunlight. Moreover, observations of spectra from plasma have contributed considerable in the development of the quantum theory. Finally, the lightning industry is fully dominated by the spectral emission of plasmas. For fusion plasmas, the beauty however lies much more in the diagnostic relevance itself: instead of learning about the atomic structure, this light comprises a wealth of quantitative information on the plasma environment itself. With appropriate background knowledge of the emission processes, quantities like the ion densities, the temperature or current distribution can be concealed from measuring the spectral intensity. Figure (1), a typical example of a spectrum in the VUV wavelength range of a tokamak is sufficient to illustrate this point. The information in the spectrum is hidden in its parameters: intensity, wavelength, spectral width and polarization. This lecture will address the basic features to relate these measurable quantities to the plasma parameters of interest. The instrumentation and techniques employed for these spectroscopy measurements will be briefly touched, as are some examples of active spectroscopic techniques. This lecture is not intended as an extensive review. Excellent textbooks are already available for that purpose (for instance [1, 2, 3, 4, 5, 6]).

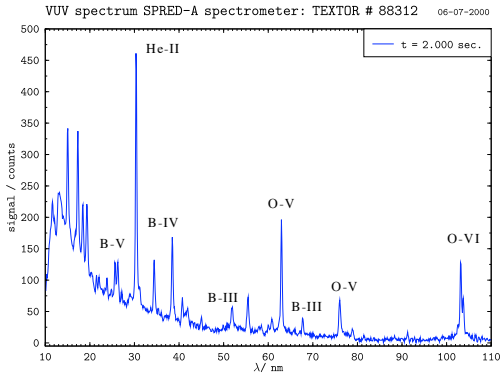

Figure 1: Typical example from TEXTOR of the spectral emission in the EUV/VUV wavelength range, for a standard ohmic discharge after boronisation. From W. Biel-FZJ

II. RADIATIVE PROCESSES

Plasma spectroscopy deviates from atomic physics in the fact that it is not the atomic structure of primary relevance but the dependence of the emission on the plasma conditions, i.e. the environment of the radiating atom. Therefore, here we assume the electronic energy structure of the atoms (or ions or molecules) for granted. Just as a short reminder, for the simplest case of an electron in a central field of a nucleus of charge Z, the energy levels $E_n$are given by the Rydberg formula:

$$E_n = R_y Z^2/n^2 \qquad (1)$$

with R_y is the Rydberg constant and n the principle quantum number. For more electron systems, the same still holds if n is replaced by $n_{eff} = n - d$, d being the quantum defect. For molecules, the energy associated with vibrational or rotational motion adds to the energy in Eq. 1. External electric and magnetic field might also contribute to changes in the energy levels (Zeeman and Stark effect), leading in general to complicated energy level diagrams. A transition between

two levels E_i and E_j will be accompanied by the emission ($E_i > E_j$) or absorption ($E_i < E_j$) of a photon with a frequency v_{ij} given by:

$$hv_{ij} = E_i - E_j \tag{2}$$

In a plasma the atoms and ions will undergo transitions between these states through different radiative and collisional processes. In general the radiative processes include spontaneous decay, absorption, stimulated decay, all between bound states and recombination transition of free electrons into a bound state. Collisional processes include electron impact excitation / de-excitation, impact ionization and three body recombination. The spectral intensity distribution of the plasma depends on the population density of the energy levels, which in turn depends on the relative weights and cross-sections of these processes. Whereas in general this collisional radiative model is a quite complex system, some limiting case are discussed here to give a flavor of the essential ingredients. The first case is the complete thermal equilibrium. Then the radiation field has reached the blackbody level (so emission and absorption are in equilibrium) and the atoms adopt the Boltzmann distribution between all possible states. In practice, the radiation field is rather weak and this situation is essentially never reached. Local thermal equilibrium (LTE) is less restrictive. Here the condition for the radiation to be thermal is dropped. For LTE all population and depopulation processes are in equilibrium with their reverse processes. Also in this case the relative population of states of on atom or ion is given by the Boltzmann distribution:

$$n_i/n_j = g_i/g_j \exp\left(-\Delta E_{ij}/kT\right) \tag{3}$$

Where $g_{i,j}$ are the statistical weights of the states participating in the transition. For LTE the densities of the successive ionization stages is then given by the Saha equation:

$$\frac{n_e n_{i+1}}{n_i} = \frac{g_{i+1}}{g_i}\left[\frac{2m_e^3}{h}\left(\frac{2\pi T}{m_e}\right)^{3/2}\right]\exp\left(-\frac{\chi_i}{kT}\right) \tag{4}$$

where χ_i the ionization potential. Also this distribution holds only for high densities or for high quantum numbers, i.e. not the situation we are normally interested in when diagnosing fusion plasmas. For those conditions the so-called Corona model is a good approximation. The basic assumption here is that all transitions to higher levels are collisional (i.e. electron impact excitation, impact ionization or dielectronic recombination) and to lower levels are radiative (decay or recombination). So absorption effect or collisional de-excitation is negligible, which holds for low enough densities. For this corona equilibrium one obtains the following relation between the different ionization stages:

$$\frac{n_{i+1}}{n_i} \approx 10^8 \frac{\zeta}{n_0}\frac{1}{\chi_i^2}\frac{kT}{\chi_i}\exp\left(-\frac{\chi_i}{kT}\right) \tag{5}$$

with ζ the number of electrons in the outer shell. As an application of the Saha and coronal equation, Figure 2 shows the relative carbon line intensities for different ionization stages as a function of the temperature. This figure illustrates the differences in emission depending on the population processes. In case of coronal equilibrium the temperature required for a line to appear is considerably larger than in thermal equilibrium (Saha). Since the temperature is a radial profile in a tokamak, an accurate treatment of the distribution of the ionization stages is also necessary for a radial localization of the radiation.

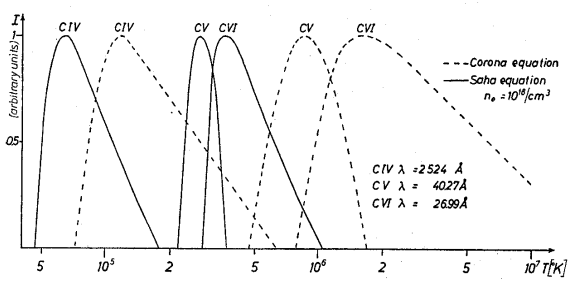

Figure 2: Relative carbon line intensities for different ionization stages as a function of temperature calculated form the Corona model and the thermal equilibrium. From [7]

.

The more important use of the collisional radiative modeling (or its simplification of the coronal assumption) is the conversion of measured intensities to ion densities of fluxes. The excited state density can be directly obtained from the measured line intensity, provided the Einstein coefficient A_{ij} for the transition from state i to j is known. To relate this to the density of the ground state, the parameter of interest, an appropriate model (e.q. corona equilibrium, LTE, etc.) is needed. The determination of the particle confinement time τ_p from the flux Φ_A serves as an illustrative example. The emission coefficient ϵ for the transition of an upper level i to a lower level j is defined by:

$$\epsilon = \frac{1}{4\pi} n_A^* A_{ij} \tag{6}$$

where n_A^* is the density of the excited state of ion A. What we are interested however is the density of the ground state n_A instead of n_A^*. Now, for the corona equilibrium, the collisional excitation into the excited

levels from the ground state can be related to the radiative decay to all lower levels:

$$n_A^* \sum_{k<i} A_{ik} = n_A n_e \langle \sigma_{ex} v_e \rangle \tag{7}$$

Here $\sum A_{ik}$ is the transition probability from level i into all lower states k and $\langle \sigma_{ex} v_e \rangle$ the excitation rate coefficient by electron collisions from the ground state (a function of T_e). The branching ratio is defined by $\Gamma = A_{ij} / \sum_{k<i} A_{ik}$. Using this we find for the measured intensity I_{tot}:

$$I_{tot} = h\nu \int_{r_1}^{r_2} \epsilon dr = \frac{h\nu\Gamma}{4\pi} \int_{r_1}^{r_2} n_A(r) n_e(r) \langle \sigma_{ex} v_e \rangle \, dr \tag{8}$$

Returning now to the parameter of interest, Φ_A, the flux of atoms into the plasma. Assuming that all atoms are ionized on their way into the plasma, one may readily obtain: $\Phi_A = n_a n_e \langle \sigma_i v_e \rangle$, with σ_i the ionization cross-section and n_a the neutral density of the atoms. Inserting this into eq. 8, relates the flux to the measured intensity:

$$\Phi_A = \frac{4\pi I_{tot}}{h\nu\Gamma} \frac{\int_{r_1}^{r_2} n_a n_e \langle \sigma_i v_e \rangle \, dr}{\int_{r_1}^{r_2} n_a n_e \langle \sigma_{ex} v_e \rangle \, dr} \approx \frac{4\pi I_{tot}}{h\nu} \frac{S}{XB} \tag{9}$$

with $S \equiv \langle \sigma_i v_e \rangle$, $X \equiv \langle \sigma_{ex} v_e \rangle$ and $B \equiv \Gamma$. For expression (9) the assumption is made that the ratio of the cross-sections do not vary appreciably over the observed region. The ratio $S/(XB)$ represents the ionization events per photon and includes all the relevant rate coefficients from the collisional radiative modeling. Suitable packages exists for these calculations, like ADAS [8]. The final step now to arrive at the particle confinement time in steady state is by integrating the flux over the outer surface of the plasma:

$$\tau_p \equiv N_a / \Phi_A^{tot} = \frac{h\nu}{16\pi^3 aR} \left(\frac{XB}{S} \right) \frac{N_A}{I_{tot}} \tag{10}$$

where in the case of hydrogen the assumption can be made that $n_A \approx n_e$, the total number of electrons.

III. OPACITY

In the description above we have tacitly assumed that absorption of radiation is negligible. If spontaneous decay from an upper level to a lower level occurs, the reverse process, absorption of the same photon by the lower level is possible as well. To quantify this, one can calculate the absorption coefficient κ_ν, defined as the absorbed fraction of radiation I^0 per unit length x [3]:

$$\kappa_\nu = \frac{dI_\nu(x)}{dx} \frac{1}{I_\nu^0(x)} = \frac{e^2}{4m_e c\epsilon_0} n_l f_{lu} P(\nu) \tag{11}$$

The last equality relates the cross section for absorption to the oscillator strengths f_{lu} (related to the Einstein coefficients A_{ul}) and the density of the absorbing particles n_l. In this equation $P(\nu) = P(\lambda)c/\lambda^2$ represents the normalized line shape. For a Doppler broadened line (see below), we can rewrite this as a mean free path of the photon mfp_λbefore it gets absorbed as:

$$\begin{aligned} mfp_\lambda = (\kappa_\lambda)^{-1} &= \frac{4m_e\epsilon_0 c}{e^2} \sqrt{\frac{2kT_i}{m_i}} \Big/ \left(n_l f_{lu} \lambda_0 \sqrt{\pi} \right) \\ &= 5 \times 10^{17} \frac{\sqrt{T_e\,[eV]}}{n_1\,[m^{-3}]}\,[m] \end{aligned} \tag{12}$$

Where in the last equality the values for the Lyman-α line ($\lambda_0 = 122nm$, $f_{12} = 0.4162$), have been used. Only in that case the density of the ground state, neutral hydrogen, is sufficiently large that the opacity might be noticeable: In the divertor for a typical neutral density of $n_H = O(10^{20} m^{-3})$ absorption of the light is expected within a few cm. For almost all other transitions, the absorption can be neglected (justifying the assumption that the plasma is not in thermal equilibrium).

IV. LINE BROADENING

Next to the intensity, the other directly accessible spectral characteristic to be measured is the line width. The width of a spectral line is governed by three different processes: the natural line width, Doppler Broadening and pressure broadening. The natural line width, related to the finite lifetime of an excited state as characterized by the Einstein coefficient A ($\Delta\lambda \approx \lambda^2 A_{ij}/(\pi c)$), is in all practical case negligible in a fusion plasma. The Doppler effect on the contrary, is the dominant mechanism for line broadening. Applying the Doppler effect over the Maxwellian ion velocity distribution function gives rise to a Gaussian line shape $P(\lambda)$:

$$P(\lambda)d\lambda = \sqrt{\frac{m_i c^2}{2\pi k T_i \lambda_0^2}} \exp - \frac{m_i c^2 \left(\lambda - \lambda_0\right)^2}{2kT_i\lambda_0^2} \tag{13}$$

with a width (expressed here as FWHM: full width at half maximum) $\delta\lambda$:

$$\Delta\lambda_D = \sqrt{\frac{8kT_i ln2}{m_i c^2}} \lambda_0 \tag{14}$$

with k the Boltzmann constant and λ_0 the unshifted line. This equation 14 shows the ease at which spectral measurement can provide the ion temperatures T_i of the plasma. The final broadening mechanism we address here is pressure broadening, or also called Stark broadening or collisional broadening. This effect result from the fact that the radiating ions experience a change in

the electric field due to the presence of neighboring ions. Detailed calculations of this effect are extremely complicated, but for hydrogen some good approximations exist [9]:

$$\Delta\lambda_S = 0.54\alpha_{1/2} n_{20}^{2/3} nm \tag{15}$$

with $\alpha_{1/2}$ a constant resulting from the calculations ($\alpha_{1/2} \approx 0.08$ for the Balmer-β transition) and n_{20} the electron density in units of $10^{20} m^{-3}$. For typical tokamak conditions ($n_{20} < 1$), this broadening is negligible compared to the Doppler broadening, even for temperatures as low as 1 eV. Only in the divertor region densities might be sufficiently high for this to become appreciable.

V. CONTINUUM RADIATION

Up to know the discussion on the radiation was limited to transitions involving bound states of the electrons. However, the emission by free electrons deserves a prominent place as well in this discussion. In general radiation is emitted if a free particle is accelerated. This can occur as a result of an electron experiencing either an electric or magnetic field. The latter results in cyclotron radiation, associated with the gyro motion of the electron. This is left out of the discussion here, since it is treated in the microwave diagnostics part of this lecture course [10]. For the former one the dominant term is the varying electrical fields experienced by the electron moving in the Coulomb field of an ion. In case the final state of the electron is also free, this is called bremsstrahlung. If after the encounter with the ion, the free electron occupies a bound state, the radiation is referred to as recombination radiation. Both types are observed as continuum radiation, due to the free nature of the electron. The continuum spectrum extends from the plasma frequency up to the x-ray region (with photon energies of the order of the electron temperature).

The derivation of the bremsstrahlung can be done instructively by considering the power emitted by an electron during an accelerated motion and apply this to a Coulomb collision. For small impact parameters of the collision quantum mechanical effects then come into play. The final expression obtained for the emissivity per unit of frequency ϵ_ν of the continuum spectrum for one ion species Z is (see for instance [4]):

$$\epsilon(\nu) = n_e n_i Z^2 \left(\frac{e^2}{4\pi\epsilon_0}\right)^3 \frac{8\pi}{2\sqrt{3} m_e^2 c^3} \left(\frac{2m_e}{\pi T_e}\right)^{1/2} e^{\frac{-h\nu}{T_e}} \times \left[\bar{g}_{ff} + G_n \frac{\zeta}{n^3} \frac{\chi_i}{T_e} e^{\frac{\chi_i}{T_e}} + \sum_{\nu=n+1}^{\infty} G_\nu \frac{2Z^2 R_y}{\nu^3 T_e} e^{\frac{Z^2 R_y}{\nu^2 T_e}}\right] \tag{16}$$

The first term in brackets is the free-free contribution, the second the recombination term into the lowest unfilled shell (n) and the third term to all other shells. The symbols used here are: G the Gaunt factor describing the quantum mechanical effects, $\bar{g}_{ff}$ the Maxwell averaged free-free Gaunt factor, ζ the number of unfilled positions ion the lowest shell, χ_i the ionization potential and R_y the Rydberg energy(13.6 eV). Evaluating this expression shows that recombination is negligible for $\lambda >> hc/Z^2 R_y \approx 100nm$ or for all wavelengths if $T_e >> Z^2 R_y$. So in the visible the bremsstrahlung dominates the continuum radiation. Furthermore, note the square dependence on the density and the (evaluating the exponent) much weaker $T_e^{1/2}$ dependence.

Apart from an additional power loss term for the plasma, the practical use of the bremsstrahlung measurement lays in the diagnostic application: plotting the continuum over a broad wavelength range on a logarithmic scale allows to deduce the electron temperature directly from the slope of the plot. Furthermore another primary quantity that can be obtained from these bremsstrahlung measurement is the effective ionic charge of the plasma, Z_{eff}. By summing the emission from eq. 16 over all ionic species and invoking quasi neutrality ($n_e = \sum n_i Z_i$), Z_{eff} is defined as the factor over which the bremsstrahlung exceeds that of hydrogen, and thus can be regarded as a kind of mean ionic charge of the plasma:

$$\sum_i n_e n_i Z_i^2 \equiv n_e^2 Z_{eff} \Rightarrow$$
$$Z_{eff} = \sum n_i Z_i^2 / \sum n_i Z_i \tag{17}$$

These measurements are usually done in the visible wavelength range, due to the relatively less cumbersome absolute calibration effort. Precaution should be taken however, to select a wavelength range free of line radiation from atoms, ions or molecules.

VI. ACTIVE DIAGNOSTICS

Contrary to this passive emission, active techniques can be used to induce specific radiation, leading to even more detailed information. One of the main reasons to use active spectroscopy is that it can access the core of the fusion plasmas. At the high temperatures required for the fusion process all the light elements in the core are fully ionized and do not emit any line radiation. By active techniques, spectral emission can be induced, and as such measurements of, for instance, the temperature from the Doppler shift is still possible. Typical examples here are the use of lasers or atomic beams. From the laser aided diagnostics, two techniques are considered here: laser induced

fluorescence, LIF and the scattering of radiation by the electrons in the plasma: Thomson scattering, TS. Beam aided spectroscopy will be examplified by charge exchange recombination spectroscopy, CXRS and Beam Emission Spectroscopy (including Motional Stark Spectroscopy).

VI.A. Laser Induced Fluorescence

The LIF technique is based on the excitation of atoms (or ions or molecules) by the absorption of laser radiation, and the measured spontaneous emission of the subsequent decay (either to the same level or to another level). To illustrate the principle of LIF, consider the simplest scheme of a two-level system (see also [12]). Then the rate equation for the excited state population is given by:

$$\frac{dN_2}{dt} = N_1 \left(W_{12} + Q_{12}\right) - N_2 \left(W_{21} + Q_{21} + A_{21}\right) \quad (18)$$

with $N_{1,2}$ the population of the lower and upper lever respectively, and $W_{12,21}$ the laser-induced absorption and stimulated emission rate, $Q_{12,21}$ the collisional excitation rate and quenching rate and A_{21} the spontaneous emission rate. It is clear that even in steady state, it is non-trivial to relate the fluorescence signal (proportional to A_{21}) to the number of electrons in the excited level N_2. For sufficiently strong lasers power densities S_p, the absorption and stimulated emissions (W) become so large that the N_2 population approaches saturation. This requirement on the laser power needed to reach this saturation is then determined by the condition that the stimulated absorption rate equals the spontaneous emission, which typically amount to $10kW/cm^2$. In this saturation limit, one finds:

$$n_{ph} = \frac{\left(N_1 + N_2\right) g_2 k}{g_1 + g_2} A_{21} \quad (19)$$

where n_{ph} is the number of fluorescence photons per s, $g_{1,2}$ the statistical weights of the two levels and

$$k = \frac{V \tau \Delta\Omega}{4\pi} \quad (20)$$

a geometrical factor consisting of V the sampling volume, τ the transmission of the collection optics, and $\delta\Omega$ the solid angle.

Although the above is an oversimplification of the real system, it demonstrates the main principle. The main advantages of this LIF technique over usual passive spectroscopy are at least two-fold. The first arise from the ability to localize the region of the measurement by crossing the laser line with the viewing optics. Second is the advantage of detecting signals which otherwise would be lost in a large background. LIF has been used in fusion research to determine several parameters like neutral densities [13], ion densities and velocities or magnetic fields [14]. A typical setup is shown in Fig. 3.

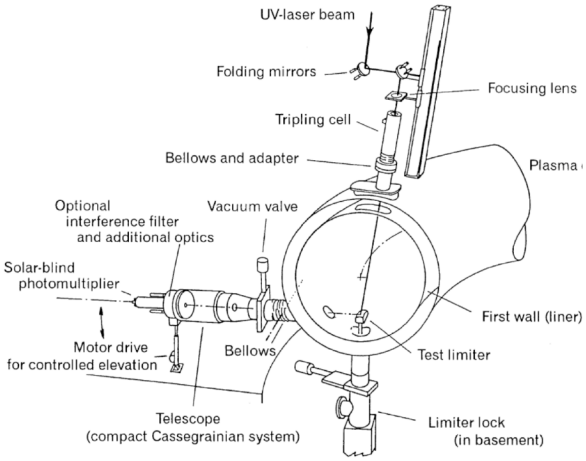

Figure 3: Experimental setup for LIF on TEXTOR edge plasma [15].

VI.B. Thomson Scattering

Thomson scattering is one of the most basic and common diagnostics at nearly every magnetic confinement device. Usually if provides profiles of electron temperature and density, but additional information, like the fast ion density or current density can be obtained as well from it, depending on arrangement of the system. Contrary to the sections before, where the radiation from the plasma itself was discussed, here the principle of the system is based on the scattering of electromagnetic waves by free electrons. This process was theoretically described by as early as 1903 by Thomson [16] and one of the first demonstrations to a tokamak was given in 1969 at the Russian tokamak T3 [17].

Scattering of monochromatic electromagnetic radiation from hot electrons in a plasma leads to a spectral broadening of the light due to the Doppler effect. Depending on the wavelength of the incident light, the scattering on individual electrons can be added or collective effects due to the correlated interactions between the plasma electrons have to be taken into account. The criteria to determine which regime applies is given by the Salpeter parameter α [18]:

$$\alpha = \left(k\lambda_D\right)^{-1} = \frac{\lambda_0}{4\pi\lambda_D sin(\theta/2)} \quad (21)$$

where $\lambda_D = 7.4 \times 10^3 \sqrt{T_e[eV]/n_e[m^{-3}]}$ is the Debye length, k the scattering vector and θ the angle between incident and scattered wave. For $\alpha << 1$ the resulting

spectrum is determined by the scattering of individual electrons. This type is referred to as incoherent Thomson scattering. For $\alpha \geq 1$ the scattering from different electrons and their surrounding field will add up coherently, since their is a negligible phase difference between them. This is coherent Thomson scattering and although scattering takes place on the electrons, since they are surrounding the ion in the Debye sphere, information on the ion can be extracted from the scattered signal [19, 20]. A third regime is given by $\alpha \sim O(10)$. In that case $\lambda_0 sin(\theta/2)$ is of the same order as the correlation length of the density fluctuations in the plasma (of the order of the ion Larmor radius) and the collective motion of the electrons can be observed [21]. Plenty of excellent review and lecture papers on Thomson scattering exist, including the collective effects [12, 4]. Therefore we concentrate in the remainder only on the basics of incoherent Thomson scattering, by far the most applied system.

The differential Thomson cross section can be derived by considering the acceleration experienced by an electron under the action of the electromagnetic field of an incident wave. For the common case of linearly polarized incident light, this leads to:

$$\frac{d\sigma_T}{d\Omega} = r_0^2 \sin^2 \phi \tag{22}$$

with $r_0 = e^2/(4\pi\epsilon_0 m_e c^2)$ the classical electron radius. This shows immediately the small value of the cross-section ($8 \times 10^{-30} m^{-2}$) and the fact that the scattering is maximum in a plane perpendicular to the incident $\mathbf{E_0}$ ($\phi = 90°$). The scattered laser power is then given as:

$$P_s = P_0 \frac{d\sigma_T}{d\Omega} \sin^2 \phi n_e \Delta L \Omega S(k, \omega) \tag{23}$$

with P_0 the incident power, ΔL the length of the scattering volume and $S(k, \omega)$ the form factor describing the frequency shift resulting from the electron motion (and also the correlation effects in case of coherent scattering). For the case of a Maxwellian distribution function this form factor becomes for the incoherent case:

$$S(\lambda_s) = \frac{1}{\Delta\lambda_e \sqrt{\pi}} \exp - \left(\frac{\lambda_s - \lambda_0}{\Delta\lambda_e} \right)^2 \tag{24}$$

Here λ_s is the wavelength of the scattered radiation and $\Delta\lambda_e$ the 1/e width of the resulting spectrum:

$$\Delta\lambda_e = \frac{2\lambda_0}{c} \sin(\frac{\theta}{2}) \sqrt{\frac{2k_b T_e}{m_e}} = 1.94\sqrt{T_e[eV]} \ [nm] \tag{25}$$

In the last expression the values for a ruby laser (λ_0=694.3 nm) and perpendicular scattering have been inserted. Note that the above derivation has neglected relativistic effects. However, for plasmas of typically 1-10 keV they become important due to two effects: the Thomson cross-section is appreciably decreased due to the mass defect by the factor $1/\gamma^2$ and the fact that the electron radiates preferentially in the forward direction(the "headlight" effect). An analytical description of this is provided by [22] and gives rise to distortion of the Gaussian spectrum, most apparent as a blueshift of the spectrum.

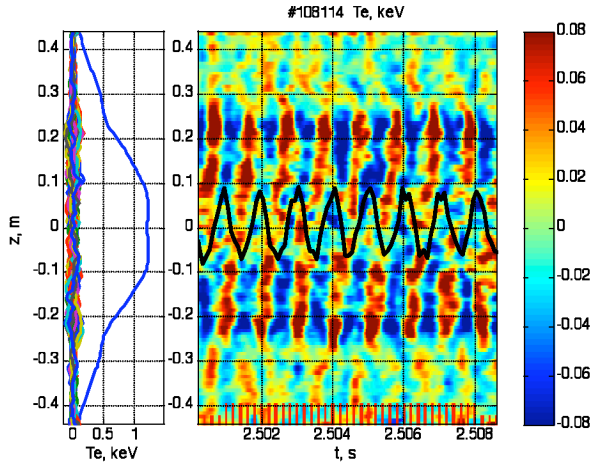

Figure 4: Typical result of the TEXTOR Thomson scattering system. Depicted here is the temperature evolution of magnetic islands in the plasma. The averaged profile (left) has been subtracted. The black line indicates the rotation of islands as measured with ECE. Temperature structures as small as 10 eV can be recognized (on a 1.5 keV background).

Several different Thomson scattering system are in use nowadays: (1) using repetitive lasers in combination with filter spectrometers to achieve relatively high temporal resolution. Since the Thomson scattering cross-section is so low (ratio of detected power over incident power is about 10^{-15}, (see Eq./ 23) strong lasers are required, with only a limited repetition frequency. However by packing several of these lasers (e.g. Nd:YAG lasers at 30 Hz) together and firing them independently, still high temporal resolutions can be achieved [23]. (2) LIDAR, which is based on a time of flight measurement of the back-scattered light of a short laser pulse. Presently only one such system is operational, at JET [24], but it is envisaged to develop such a system as well for ITER, since it has the big advantage that only one access window for both the laser and collection optics is required. (3) TV systems, which image the full laser cord on a CCD or CMOS cameras and thus have an excellent spatial resolution of less than a cm. Most advanced system in this respect is the TEXTOR Thomson system. Here the plasma is part of the laser cavity, allowing the operation of a multi pulse ruby laser at sufficiently high power. By adjusting the laser

path such that the laser pulse can travel up to 12 times through the plasma typically a burst of 60 pulses at 5 kHz repetition frequency and 60 J of effective laser power can be reached [25]. This high power, combined with the high spatial and temporal resolution allows to observe the dynamic of small structures in the plasma, like the rotation of magnetic islands, see Fig. 4.

VI.C. Charge eXchange Recombination Spectroscopy

The exchange of an electron between a hydrogen neutral and fully ionized particles is a resonant process which has its maximum cross section in the energy range of a few tens of keV for the light ions (H,He,B,Be,C,N,O,Ne, Ar) that are typically encountered in the tokamaks. In this energy range (10-100 keV) it is the dominant ionization process of neutral beams heating the plasma. These heating beams can thus be also be used to induce line radiation from the plasma core. For an arbitrary plasma ion X capturing the electron from the hydrogen neutral beam, the reaction is written as:

$$\begin{aligned} H_{beam} + X^{Z+} &\rightarrow H^+_{beam} + X^{(Z-1)+}(n_1) \\ &\rightarrow H^+_{beam} + X^{(Z-1)+}(n_2) + h\nu_{12} \end{aligned} \quad (26)$$

where $h\nu_{12}$ representing the photon due to the radiative decay from the excited level n_1 to the level n_2. The thus emitted spectrum entails the information from the core ions: its width squared propotional to the ion temperature (14), the Doppler shift to the core rotation along the line of sight and the intensity proportinal to the ion density. Apart from the bare fact that this method allows to access the fusion core at all, the other big advantage of this method is that it is a local measurement: the recorded emission originated from the intersection of the neutral beam and the line of sight. This allows to obtain ion temperature, ion rotation and ion density profiles over the full plasma radius. Furthermore, the principle shell into which the electron will be caught can be approximated by $n_2 \approx Z^{3/4}$ for CX from the ground state (see [4]). For light elements like Carbon and Neon higher levels are populated, which allows transitions into the visible wavelength region, making the recording relatively easy. For helium this is only true to certain extent. A typical example of a carbon spectrum in shown in Fig. 5. (Note: carbon is usually used due its relatively uncomplicated spectral shape and its presence in all plasmas, since carbon is used as the most common wall material and thus diffuse into the core plasma. For future reactors, this might not be the case, since carbon has to be avoided because of its tritium retention capability). Over the past three decades the CXRS diagnosic has been developed to an extent that it is now the main core ion diagnostic [26].

For ITER a dedicated diagnostic neutral beam system (with an energy of 100 keV) is envisaged, since CXRS is the sole possibility to diagnose the helium ash density in the core [27].

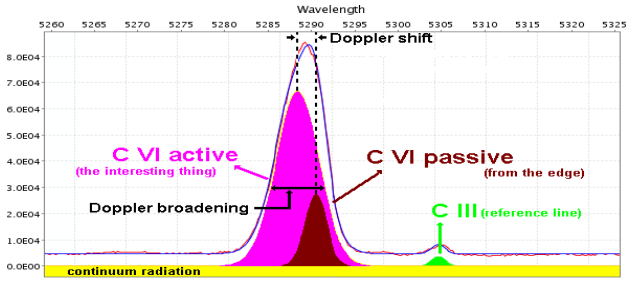

Figure 5: Typical carbon spectrum of the TEXTOR Charge Exchange Recombination System. The measured line originated from $C^{5+}(n = 8 \rightarrow n = 7 at \lambda = 529nm$. Without the neutral beam, only a passive line originating from the plasma edge is observed. When the beam is switched on the active component appears: its width being representative of the carbon temperature, its Doppler shift is related to the ion rotation along the line of sight and the intensity is a measure of the carbon density.

Complications with this method arise mainly from two issues: i) apart from the active CX components, also emission from the same passive line, coming from the cold edge plasma, appears. This emission is always present, and originated either from CX reactions with neutrals from the wall instead of the beam or from the impact excitation of the non-fully stripped ion $X^{(Z-1)+}$ in the plasma edge. Discrimation between the active and passive components can be done by a modulated neutral beam (as envisaged for ITER) or by a (cumbersome) fitting procedure. ii) the neutral beam is attenuated towards the plasma centre (due to the ionization processes, of which CX itself is the dominant one). For large plasmas this makes the signal rather weak in the centre. For ITER, where only 1% of the beam particles arrive in the centre, this can be compensated only by a large light collection system. The beam attenuation complicates also the derivation of the ion density from the intensity signal (proportional to $n_X n_{beam}$). An accurate knowledge of the beam density in the observed volume is thus required and can be obtained from attenuation codes (calculating the integrated beam ionization along the beampath) or from measuring the beam density directly from the direct emission from the beam itself (i.e. the beam excitation by electron/ion impact collisions). Both methods rely on atomic cross-section of the relevant processes, which are still subject to investigations or validation [28].

VI.D. Beam Emission Spectroscopy

Detecting the emission from the neutral beam itself has three interesting applications: Firstly, the determination of the beam density, as discussed in the previous section, with the aim to obtain the ion density profile from CXRS measurements. Secondly, the fluctations in the intensity of the beam emission is related to the fluctuations on the electron density. On DII-D a 2D system based on this measurement has been constructed, which showed both the fluctuation levels as the flows of the tubulent structures in the plasma [29]. However, the most renown application of the beam emission is related to the Motional Stark Effect (MSE). The fast beam neutrals, moving in an large magnetic field, experience a Lorentz electric field in their reference frame ($\mathbf{E} = \mathbf{v_{beam}} \times \mathbf{B}$), which gives rise to a Stark splitting of their energy levels. A typical example of such hydrogen beam spectrum at the Balmer-α transition is given in Fig. 6. From the Stark splitting ($\sim E$), or the polarisation ($\sim$ direction of E), information on the amplitude or direction of the magnetic field ($\mathbf{B}$) can be obtained, since $\mathbf{v_{beam}}$ is accurately know. Typical MSE diagnostics employ an interference filter to select one component from the spectra with an polarisation direction parallel or perpendicular to $\mathbf{B}$. Measuring the polarisation angle of this line then determines the magnetic field direction, which is used as input parameter to the plasma equilibrium codes, constraining the current density profile [30].

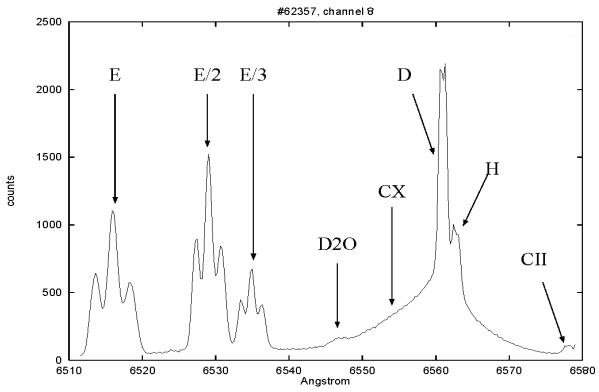

Figure 6: Typica spectrum of the Balmer-α emission of a Neutral Beam Heated discharge at TEXTOR. The Blue shifted Doppler lines originate from Balmer $n = 3 \rightarrow n = 2$ emission, which is splitted due to the motional Stark effect. This emision is polarised eitehr parallel or perpendicular with respect to the Lorentz electric field $E_L = v \times B$. (The three separate groups are due to the different energy species in the neutral beam at 50, 25 and 16.7 keV)

VII. INSTRUMENTATION

Key to the success of the plasma spectroscopy is the instrumentation. The choice of the instrument depends heavily on the wavelength of interest. Typically one can distinguish: a) the visible range ($h\nu \sim 2-3eV$), mainly for passive spectroscopy in the plasma edge, since only their the temperature is low enough that the atoms or ions exhibiting these low energy transition are available, 2) the UV/VUV range ($h\nu \sim 3 - 120eV$) typical of higher ionization stages of impurity ions as they occur in the confined region of the plasma and 3) X-ray measurements ($h\nu \sim 0.12 - 10keV$), typical of highly charged states as they occur in plasma regions of 1 keV or more, so sensitive to the core of the plasma. For all these ranges, a spectral instrument should obey the following characteristics: a high resolving power $R = \Delta\lambda/\lambda$ to discriminate the different lines, high light transmission T and good imaging quality. The most used types in all ranges are grating spectrometers, as they can combine all these properties simultaneously. Prism instruments, Fabry-Pérot inerferometer and Fourier transform spectrometers are used only for special purposes.

VII.A. Spectrometer

The dispersion of a grating spectrometer is governed by the grating equation:

$$m\lambda = d(\sin\alpha + \sin\beta) \tag{27}$$

with m the diffraction order, d the line separation and α, β the angles of the incident and reflected light respectively. The resolving power is then determined by the total number of illuminated lines N: $R = Nm$. Densities of 6000 lines/mm can be attained on a 10 cm grating, yielding a resolving power of 6×10^5 in the first order. The intensity of the diffracted light depends on the shape of the lines. Ruled grating are optimized (in reflectivity) with respect to a certain *blaze* angle corresponding to a certain wavelength. Efficiencies can be as high as 70 % at this wavelength. A special category are *Echelle* gratings, where one has comparatively few lines/mm but one operates this at high diffraction orders, so even achieving $R \sim 10^6$. Disadvantage there is the problem of many overlapping orders (i.e Eq. 27 fulfilled for different wavelengths at different orders m.

Another characteristic of the spectrometer is its etendue E or light throughput, representing the total light collection efficiency. It is given by the product of the area A of the entrance slit and the acceptance angle Ω, related to relative aperture $F/\#$:

$$E = A\Omega = \frac{\pi}{4}\frac{A}{(F/\#)^2}. \tag{28}$$

Since the etendue is cannot be increased in optical system, the spectrometer's etendue usually limits the light collection efficiency. To acquire a reasonably high signal to noise ratio for CXRS in the core of ITER, a high resolution, high etendue spectrometer has been designed with an unsurpassed etendue of $E = 1mm^2sr$ [31].

Spectrometers consist typically of the optics to collimate the light from the entrance slit towards the dispersive element (like the grating) and then image the dispersed light back to the exit slit where a detector might be located. Different types of optical arrangements exist, like the Czerny Turner or Littrow mount for the visible wavelength range. These are designed such to eliminate or minimize the optical aberrations and attain good image quality. If concave grating are used, the need for collimating and focussing is eliminated, which is particularly useful in the VUV en XUV regions, where conventional mirrors are ineffective. For even shorter wavelengths, the gratings are used at grazing incidence, to minimize the absorption losses. In X-ray one typically employs crystals instead of ruled gratings, where the diffraction occurs according to the Bragg condition for the atomic planes. An example is shown in Fig. 7 of a conventional Johann Crystal spectrometer [32]. More advanced present day designs have optimized this to have an imaging capability as well. This now allows to obtain profiles of ion temperature and rotation on large tokamaks [33].

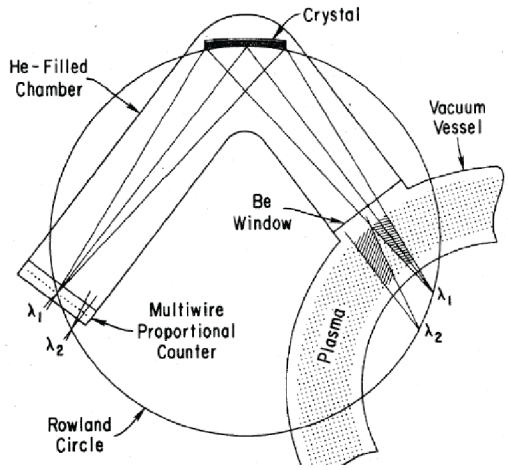

Figure 7: Example of a Johann Crystal spectrometer for application in the X-ray region. From [32]

.

VII.B. Coherence Imaging

The other alternative to obtain spectral information is by measuring the coherence of light. An example of this is a Fourier transform spectrometer, but other arrangements are possible as well. An elegant example of this was developed for instance at WEGA [34]. Such systems monitor in two dimensions the temporal coherence of an isolated spectral line using polarization interferometric techniques. For quasi-monochromatic illumination, the signal, S (interferogram), at the output ports of a two-beam interferometer is given by:

$$S = \frac{I_0}{2}(1 + \zeta \cos \phi) \tag{29}$$

where I_0 is the source brightness, ζ is the fringe contrast and ϕ is the phase delay of the interferometer. When the emission line is now broadened, i.e. with increasing temperature, the fringe visibility decreases. To observe changes to the fringe visibility, it is necessary to modulate the optical path length (phase delay) in order to extract the fringe amplitude. This modulation is achieved electro-optically using a step-modulation pattern that is synchronized with the camera frame rate. Using a fast CCD camera this system can obtain the spectrum in 2D, since the spectral information is moved to the time domain. Further extensions to this system are being explored to use it for Zeeman or Motional Stark measurements [35].

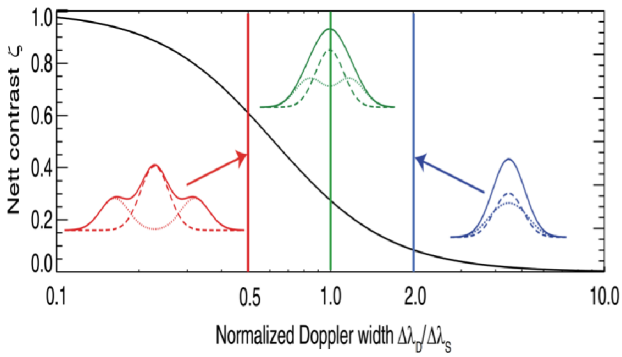

Figure 8: The calculated maximum nett contrast ζ versus the ratio of Doppler width $\Delta\lambda_D$ and Stark separation $\Delta\lambda_s$. The insets show the multiplet line-shapes for ratios 0.5, 1 and 2, corresponding to different polarization angles. (From [35])

.

ACKNOWLEDGMENTS

This paper builds upon lectures given at previous editions of the Carolus Magnus Summer School by Dr. A. Pospieszczyk (FZ-Jülich), Dr. A.J.H. Donné (FOM Rijnhuizen) and Dr. B. Schweer (FZ-Jülich) and the author is much indebted to them.

REFERENCES

1. H.R. GRIEM, *Plasma Spectroscopy*, McGraw Hill, New York, (1964).
2. H.R. GRIEM, *Principles of Plasma Spectroscopy* Cambridge University Press, Cambridge (1997).
3. T. FUJIMOTO, *Plasma Spectroscopy*, Clarendon Press, Oxford, (2004).
4. I.H. HUTCHINSON, *Principles of Plasma Diagnostics*, Cambridge University Press, Cambridge, (2002).
5. W. LOCHTE-HOLTGREVE, *Plasma Diagnostics* North-Holland, Amsterdam (1968).
6. A.A. OVSYANNIKOV, ed: *Plasma Diagnostics*, Cambridge International Science Publishing, Cambridge (2000).
7. A. POSPIESZCZYK, *Spectroscopy*, Transaction of Fusion Science and Technology **49-2T** (2006) 395.
8. Atomic Data Analysis Structure, see: http://adas.phys.strath.ac.uk.
9. H.R. GRIEM, *Spectral Line Broadening by Plasmas*, Academic Press, New York, (1974).
10. A. KRÄMER-FLECKEN, this lecture course.
11. B. SCHWEER, *Atomic Beams for Plasma Diagnostics*, this issue.
12. A.J.H. DONNÉ *Laser-aided Plasma Diagnostics*, Trans. of Fusion Science and Technology, **49-2T** (2006) 375.
13. G.T. RAZDOBARIN *et al.*, *Nuclear Fusion* **19**, 1439 (1979).
14. W.P. WEST *et al.*, *Rev. Sci. Instrum.* **57** 1552 (1986).
15. Ph. MERTENS and A. POSPIESZCZYK, *Journal of Nuclear Materials* **266-269** 884 (1999).
16. J.J THOMSON, *Conduction of Electricity though Gases* University Press Cambridge (1903) p. 268.
17. N.J. PEACOCK *et al.*, *Nature* **224**, 488 (1969).
18. E.E. SALPETER, *Phys. Rev.* **120**, 1528 (1960).
19. R. BEHN, *et al.*, *Phys.Rev. Lett.* **62** 2833 (1989).
20. H. BINDSLEV *et al.*, *Phys. Rev. Lett* **83** 3206 (1999).
21. A. SEMET, *et al. Phys. Rev. Lett.* **45** 445 (1980).
22. A.C. SELDEN *Phys. Lett.* **79A** 5 (1980).
23. R. SCANNELL, *et al. Rev. Sci. Instrum.* **79** 10E730 (2008).
24. C.W. GOWERS, *et al. Rev Sci. Instrum.* **66** 471 (1995).
25. M.Yu. KANTOR, *et al.*, *Plasma Physics and Controlled Fusion* **51** 055002 (2009).
26. R.C. ISLER, *Plasma Physics and Controlled Fusion* **36** 171 (1994).
27. D. THOMAS, *et al.*, *Fusion Science and Technology* **53** 487 (2008).
28. E. DELABIE, *et al.*, *Plasma Physics and Controlled Fusion* **52** 125008 (2010).
29. G. MCKEE, *et al.*,*Rev. Sci. Instrum.* **74** 2014 (2003).
30. D. WROBLEWSKI and L.L. LAO *et al.*,*Rev. Sci. Instrum.* **63** 5140 (1992).
31. W. BIEL, *et al.*, *Fusion Engineering and Design* **86 (6-8)** 548 (2011) .
32. G. BERTSCHINGER, *et al.*, *Physica Scripta* **T83** 132 (1999).
33. A. INCE-CUSHMAN, *et al.*,*Rev. Sci. Instrum.* **79** 10E302 (2008).
34. J. CHUNG, *et al.*, *Plasma Physics and Controlled Fusion* **47** 919 (2005)
35. J. HOWARD, *et al.*, *Plasma Physics and Controlled Fusion* **50** 125003 (2008)